

# The interplay between chemical and mechanical feedback from the first generation of stars

Umberto Maio,<sup>1</sup>★ Sadegh Khochfar,<sup>1</sup> Jarrett L. Johnson<sup>1</sup> and Benedetta Ciardi<sup>2</sup>

<sup>1</sup>Max-Planck-Institut für extraterrestrische Physik, Giessenbachstraße 1, D-85748 Garching bei München, Germany

<sup>2</sup>Max-Planck-Institut für Astrophysik Physik, Karl-Schwarzschild-Straße 1, D-85748 Garching bei München, Germany

Accepted 2011 January 31. Received 2011 January 28; in original form 2010 November 12

## ABSTRACT

We study cosmological simulations of early structure formation, including non-equilibrium molecular chemistry, metal pollution from stellar evolution, transition from Population III (PopIII) to Population II (PopII) star formation, regulated by a given critical metallicity, and feedback effects. We perform analyses of the properties of the gas, and use the PopIII and PopII populations as tracers of the metallicity. This allows us to investigate the properties of early metal spreading from the different stellar populations and its interplay with pristine molecular gas, in terms of the initial mass function and critical metallicity. We find that, independently of the details about PopIII modelling, after the onset of star formation, regions enriched below the critical level are mostly found in isolated environments, while PopII star formation regions are much more clumped. Typical star-forming haloes, at  $z \sim 15-10$ , with masses between  $\sim 10^7$  and  $10^8 M_{\odot}$ , show average supernova (SN) driven outflow rates of up to  $\sim 10^{-4} M_{\odot} \text{ yr}^{-1}$  in enriched gas, initially leaving the original star formation regions almost devoid of metals. The polluted material, which is gravitationally incorporated in overdense environments on time-scales of  $\sim 10^7$  yr, is mostly coming from external, nearby star-forming sites ('gravitational enrichment'). In parallel, the pristine-gas inflow rates are some orders of magnitudes larger, between  $\sim 10^{-3}$  and  $10^{-1} M_{\odot} \text{ yr}^{-1}$ . However, thermal feedback from SN destroys molecules within the pristine gas hindering its ability to cool and to condense into high-density star-forming regions. Only the polluted material incorporated via gravitational enrichment can continue to cool by atomic fine-structure transitions on short time-scales, short enough to end the initial PopIII regime within less than  $10^8$  yr. Moreover, the interplay between the pristine, cold, infalling gas and the ejected, hot, metal-rich gas leads to turbulent Reynolds numbers of the order of  $\sim 10^8-10^{10}$ , and contributes to the suppression of pristine inflow rates into the densest, star-forming regions.

**Key words:** galaxies: formation – galaxies: high-redshift – cosmology: theory – dark ages, reionization, first stars – early Universe.

## 1 INTRODUCTION

One of the most outstanding problems in astrophysics is the study of the birth and evolution of cosmic structures, from early times to present days. Our basic understanding relies on the observations of a Universe expanding at a present-day rate ( $H_0$ ) of  $\sim 70 \text{ km s}^{-1} \text{ Mpc}^{-1}$ , in which the baryonic content ( $\Omega_{0b}$ ) is only a small fraction ( $\sim 4$  per cent). A form of unknown 'dark' matter represents, instead, the bulk of the matter content ( $\Omega_{0m}$ ), with roughly  $\sim 23$  per cent the total energy density of the Universe. The remaining  $\sim 70$  per cent is accounted for by the contribution of the so-called 'cosmological constant',  $\Lambda$ , or 'dark energy' ( $\Omega_{0\Lambda}$ ). Re-

cent determinations of the cosmological parameters (e.g. Komatsu et al. 2011) suggest  $H_0 = 70 \text{ km s}^{-1} \text{ Mpc}^{-1}$  ( $h = 0.70$  if expressed in units of  $100 \text{ km s}^{-1} \text{ Mpc}^{-1}$ ),  $\Omega_{0m} = 0.272$ ,  $\Omega_{0b} = 0.0456$  and  $\Omega_{0\Lambda} = 0.728$ . The power spectrum of the primordial perturbations follows an almost linear scaling, with an index  $n = 0.96$  and a normalization via mass variance within  $8 \text{ Mpc } h^{-1}$  radius  $\sigma_8 = 0.8$ . As a reference, it is common to define the standard  $\Lambda$  cold dark matter ( $\Lambda$ CDM) model as the one with the following parameters:  $H_0 = 70 \text{ km s}^{-1} \text{ Mpc}^{-1}$ ,  $\Omega_{0m} = 0.3$ ,  $\Omega_{0b} = 0.04$ ,  $\Omega_{0\Lambda} = 0.7$ ,  $\Omega_{0\text{tot}} = 1.0$ ,  $\sigma_8 = 0.9$ ,  $n = 1$ . Stars and galaxies are thought to be born in such a cosmological setting (e.g. Gunn & Gott 1972; Peebles 1974). It is believed that the first stars have formed from collapse of primordial, metal-free gas (e.g. Galli & Palla 1998; Bromm, Coppi & Larson 1999; Abel, Bryan & Norman 2000, 2002; O'Shea & Norman 2007; Cen & Riquelme 2008; Yoshida, Omukai &

★E-mail: umaio@mpe.mpg.de

Hernquist 2008), and they have subsequently polluted the surrounding medium by ejecting the metals produced in their cores. This process is responsible for the cosmic metal pollution and the appearance of the first metals in the Universe. In addition, the modalities of the following star formation are altered by the enhanced cooling capabilities of metal-enriched gas. Indeed, in a primordial environment the only relevant coolants are H, He and their derived molecules (Saslaw & Zipoy 1967), like H<sub>2</sub>, HD or HeH. They are able to cool the medium only down to temperatures that result in Jeans masses  $\sim 10\text{--}100 M_{\odot}$ , and therefore present-day, common  $\sim M_{\odot}$  stars cannot be born. Metal or dust cooling (e.g. Omukai et al. 2005; Dwek, Galliano & Jones 2007; Schneider & Omukai 2010; Grassi et al. 2010; Dwek & Cherchneff 2011) and turbulence effects at the moment when the baryons become self-gravitating (e.g. Clark et al. 2011) are thought to be able to lower these limits down to solar scales, but within a large mass range.

Thus, the very first (Population III, hereafter PopIII) stars are supposed to be (e.g. Woosley & Weaver 1995; Schaerer 2002) massive, and short-lived (up to  $\sim 10^6$  yr), while the following (Population II, hereafter PopII) ones have low mass (solar-like) and can live much longer (up to  $10^9\text{--}10^{10}$  yr). Cosmological simulations addressing the role of metal enrichment in the history of the Universe have been performed, both by adopting standard recipes for star formation<sup>1</sup> (e.g. Katz & Gunn 1991; Cen 1992; Cen & Ostriker 1992; Katz 1992; Katz, Weinberg & Hernquist 1996; Springel & Hernquist 2003) and by following the detailed numerical network to account for molecular evolution and early, catastrophic run-away collapse (e.g. Gnedin 1998; Yoshida et al. 2003; Bromm, Yoshida & Hernquist 2003; Ricotti & Ostriker 2004; Wise & Abel 2008; Maio et al. 2006, 2007, 2010; Greif et al. 2010). Recent numerical simulations including both PopIII and PopII yields (Tornatore, Ferrara & Schneider 2007b) and, additionally, full molecular evolution (Maio et al. 2010) seem to suggest that the transition between the two regimes is expected to take place after the very first metal-pollution events (dominated mainly by O and C). Due to the high metal yields of primordial SN explosions, average metallicities reach  $\sim 10^{-3}\text{--}10^{-2} Z_{\odot}$  on very short time-scales (Maio et al. 2010), and the subsequent phases of the cosmic star formation history are dominated by the PopII evolution with just minor, residual contributions from the PopIII regime (e.g. Tornatore et al. 2007b; Maio et al. 2010).

Also the impacts of primordial supersonic gas bulk flows (Tseliakhovich & Hirata 2010; Tseliakhovich, Barkana & Hirata 2010) with respect to the underlying dark-matter distributions were recently studied in numerical simulations for the first time by Maio, Koopmans & Ciardi (2011), followed by Stacy, Bromm & Loeb (2010), and the conclusion was that early structure formation is suppressed, with a cascading effect inducing a time-delay in gas collapse of some  $10^7$  yr.

The detectability of the first stars has been widely discussed in the literature (for a complete review, see Ciardi & Ferrara 2005), and it is generally believed that next-generation telescopes might be able to observe the first galaxies at high redshift (e.g. Weinmann & Lilly 2005; Crowther et al. 2010; Dijkstra & Wyithe 2010; Johnson et al. 2011). An important point to stress is our ignorance about the detailed metal-pollution history at early times, when star-forming

haloes are ‘small’ (i.e. with maximum masses of the order of  $10^5\text{--}10^6 M_{\odot}$  at redshift  $z \sim 20$ , and  $\sim 10^8\text{--}10^9 M_{\odot}$  at  $z \sim 10$ ). It is reasonable that such small haloes are not able to retain all their gas, given the impact from supernova feedback (e.g. Aguirre et al. 2001; Springel & Hernquist 2003; Whalen et al. 2008). Another issue is the behaviour of pristine gas in the presence of metal-rich gas. Detailed studies of phase mixing are still needed to address this question rigorously (see e.g. Spitzer 1962; Cowie & McKee 1977; Brookshaw 1985; Sarazin 1988; Monaghan 1992; Cleary & Monaghan 1999; de Avillez & Mac Low 2002; Klessen & Lin 2003; Jubelgas, Springel & Dolag 2004; Monaghan, Huppert & Worster 2005; Wadsley, Veeravalli & Couchman 2008; Greif et al. 2009; Shen, Wadsley & Stinson 2010).

In this paper, we will outline the main features of the collapse of H<sub>2</sub>-cooled pristine gas and the subsequent pollution from early structure formation; in particular, we will address the impact of metal-rich gas on pristine, molecular gas and the interplay between the PopIII and the PopII regime. The problems we want to address are: is early metal pollution efficient in enriching the surrounding gas? How much metal mass is expelled from the star formation sites? How much metal mass is trapped in dense, star-forming environments? On which time-scales? Are metals coming from nearby star-forming regions or are they re-incorporated by the same halo where they were produced? After the first star formation episodes, can the pristine, molecular gas inflows restore the PopIII regime? Which are the preferred PopIII and PopII star formation sites? How do different PopIII initial mass functions (IMFs) influence the picture?

This work is divided as follows. In Section 2 we describe the simulations used and outline the method adopted, in Section 3 we present our results and in Section 4 we discuss and conclude.

## 2 METHODS

We use the *N*-body/smoothed particle hydrodynamics (SPH) numerical simulations presented in Maio et al. (2010), and performed by using the entropy-conserving code GADGET (Springel 2005). The code contains a complete set of the most relevant, non-equilibrium, chemical reactions (involving H, H<sup>+</sup>, H<sup>-</sup>, He, He<sup>+</sup>, He<sup>++</sup>, D, D<sup>+</sup>, HD, H<sub>2</sub>, H<sub>2</sub><sup>+</sup>, HeH<sup>+</sup>, e<sup>-</sup>), in order to properly follow the early stages of gas cooling (e.g. Yoshida et al. 2003; Maio et al. 2006, 2007, 2009, 2010, and references therein). We also include several metal species produced from stellar evolution (C, O, Si, Fe, Mg, S, Ca), according to two different populations (Tornatore et al. 2007b): the PopIII stars, described by a top-heavy IMF,<sup>2</sup> and the PopII stars, described by a common Salpeter IMF. The transition between the two regimes is determined by the critical metallicity,  $Z_{\text{crit}}$  (see also Schneider et al. 2003; Bromm & Loeb 2003). We consider several scenarios for the possible PopIII IMF, by adopting different IMF mass ranges, slopes, yields and critical metallicities. In the cases where a top-heavy IMF was assumed (see also e.g. Ricotti & Ostriker 2004; Karlsson, Johnson & Bromm 2008; Maio et al. 2010), the pollution was faster and stronger, reaching  $\sim 10^{-3}\text{--}10^{-2} Z_{\odot}$  immediately after the onset of star formation. The cases of moderate- or low-mass IMF show a similar, but more gradual, trend. Since the

<sup>1</sup> Several studies use a different way to deal with star formation, i.e. via ‘sink’ particles, but we warn the reader that very recent calculations (Bate, Lodato & Pringle 2010) have shown two main limitations of this approach: overprediction of the accretion rates and mispredictions of the particle orbits.

<sup>2</sup> The exact slope for the PopIII IMF has little effect on the metallicity evolution. The main contribution to the metallicity is via pair-instability supernovae (PISN) whose fraction only show slight changes between  $\sim 0.35$  and  $0.40$ , for variations of the slope within the limits of  $\sim [-3.0, -0.5]$ , given an IMF range of  $\sim [100 M_{\odot}, 500 M_{\odot}]$  (Maio et al. 2010).

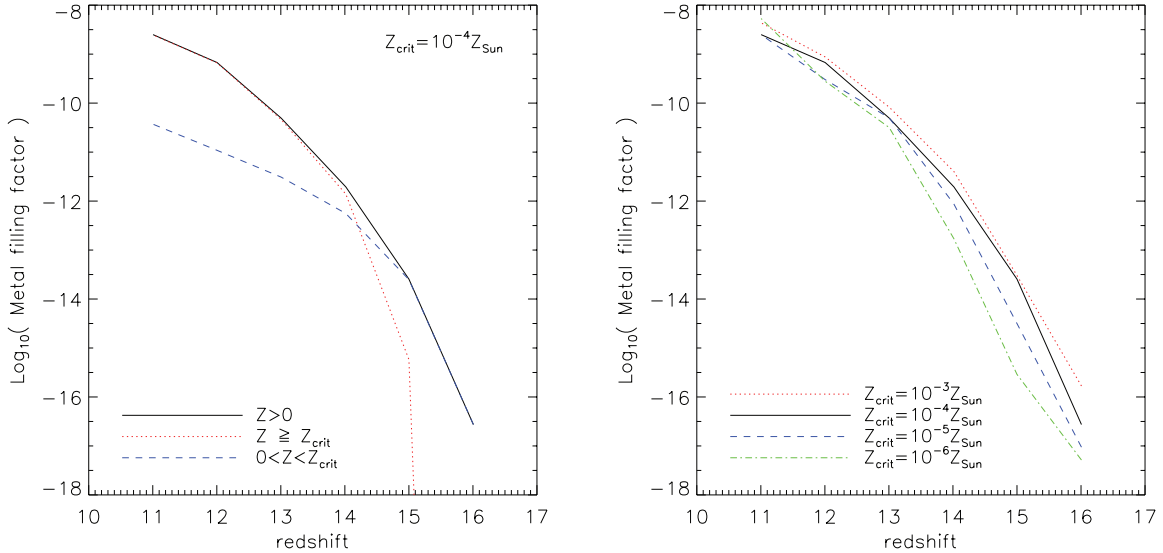


**Figure 1.** Left-hand panel: metal filling factors for different regimes. Solid, dashed and dotted lines are the filling factors computed for particles having metallicity  $Z > 0$ ,  $0 < Z < Z_{\text{crit}}$  and  $Z \geq Z_{\text{crit}}$  ( $Z_{\text{crit}} = 10^{-4} Z_{\odot}$ ), respectively. Right-hand panel: metal ( $Z > 0$ ) filling factors for simulations with different critical metallicity. Dotted, solid, dashed and dot-dashed lines refer to  $Z_{\text{crit}} = 10^{-3} Z_{\odot}$ ,  $Z_{\text{crit}} = 10^{-4} Z_{\odot}$ ,  $Z_{\text{crit}} = 10^{-5} Z_{\odot}$  and  $Z_{\text{crit}} = 10^{-6} Z_{\odot}$ , respectively.

goal of this paper is an investigation of the dynamical properties of the pollution process, without loss of generality, we will focus mainly on the top-heavy IMF runs, and we will only refer to the other runs as comparison. We consider different simulations in the framework of the cosmological standard model, assuming  $Z_{\text{crit}} = 10^{-3}, 10^{-4}, 10^{-5}, 10^{-6} Z_{\odot}$ , using high-resolution boxes of 1 Mpc a side, and  $2 \times 320^3$  particles for gas and dark matter.

The main processes which cause pristine gas to cool are particle collisions and molecule creation, with typical molecule fractions becoming larger than  $\sim 10^{-2}$  and completely dominating early gas cooling. At the bottom of the cooling branch, we assume that star formation and feedback processes occur (e.g. Springel & Hernquist 2003; Maio et al. 2009), and metals are produced from stellar evolution. The feedback processes we deal with are thermal feedback, mechanical feedback (both shocks and winds) and the chemical feedback: thermal feedback from supernovae injects entropy into the medium heating up closeby particles and destroying molecules; kinetic wind feedback is stochastically taken into account, according to Springel & Hernquist (2003), and it is responsible for removing away from the collapsing sites and spreading around gas and metals at velocities of the order of some  $\sim 10^2$  km s<sup>-1</sup>; chemical feedback rules the actual stellar IMF and leads the transition from the primordial PopIII regime to the following PopII one. In the PopIII star formation regime, the only stars contributing to metal pollution are the ones in the mass range [140 M<sub>⊙</sub>, 260 M<sub>⊙</sub>], that explode as pair-instability supernovae (PISN) after a lifetime of at most  $\sim 10^6$  yr. Their contribution to the total star formation rate (SFR) rapidly drops down  $\sim 10^{-3}$ – $10^{-4}$  (see Maio et al. 2010), and this seems consistent with what can be inferred from more recent observational analyses (e.g. Papovich et al. 2010, private communication). Given the many uncertainties on the primordial IMF (e.g. see Yoshida 2006; Yoshida, Omukai & Hernquist 2007; Campbell & Lattanzio 2008; Suda & Fujimoto 2010), we also consider the other limiting case of a Salpeter-like PopIII IMF, with mass range similar to PopII, but with metal yields consistent with those from metal-free stars (see section 4.1. in Maio et al. 2010, for further details).

In the case of PopII, the surrounding environment is polluted via Type II supernova (SNII) and Type Ia supernova (SNIa), which

occur  $\sim 10^7$ – $10^8$  and  $\sim 10^9$ – $10^{10}$  yr following the formation of their progenitor stars, respectively. Moreover, stars can loose a significant fraction of mass during their asymptotic giant branch phase. Metals are injected into the ISM and pollute it by means of stellar winds. First star formation events take place at  $z \sim 16.3$ , when the Universe is roughly  $2.4 \times 10^8$  yr old.

In the following, results from our analyses will be presented and discussed. We will refer to enriched gas particles with metallicity,  $Z$ , higher than or equal to  $Z_{\text{crit}}$  as PopII particles, while to the ones with metallicity below  $Z_{\text{crit}}$  as PopIII particles. Particles with  $Z = 0$  are referred to as pristine particles.

### 3 RESULTS

In this section we present our results, paying attention first to some global properties of metal enrichment (Section 3.1), then to the statistical (Section 3.2) and dynamical (Section 3.3) ones. We also discuss the features and the interplay between the two different stellar populations (PopIII and PopII).

#### 3.1 Volume filling factor

To have a general idea of the metal spreading process, we start presenting the basic features of the volume filling factor.

In Fig. 1 (left-hand panel), the volume filling factor of metal enriched particles as a function of the redshift is shown. The volume filling factor,  $f_V$ , is defined as follows:<sup>3</sup>

$$f_V \equiv \frac{\sum_i m_{Z,i}/\rho_{Z,i}}{\sum_j m_j/\rho_j} \sim \frac{\sum_i m_{Z,i}/\rho_{Z,i}}{V}, \quad (1)$$

with  $i$  and  $j$  integers running over the number of the enriched particles and of all the SPH particles, respectively,  $m_Z$  particle metal mass,  $\rho_Z$  metal-mass density,  $m$  particle total mass,  $\rho$  total-mass

<sup>3</sup> Here, there is no difference by defining  $f_V$  via physical or comoving quantities.

density and  $V$  simulation box volume. The solid line refers to the filling factor computed by considering only the polluted particles ( $Z > 0$ ), the dashed line refers to the particles with metallicity  $0 < Z < Z_{\text{crit}}$  (PopIII regime), and the dotted line to the particles with metallicity  $Z \geq Z_{\text{crit}}$  (PopII regime). In all the three cases, the general trend is similar: the filling factor increases as redshift decreases. This is simply due to ongoing metal pollution events at  $z \lesssim 16$ . In more detail, at early times, some metals are produced, after the first PISN explosions, and the production sites are the very dense, clumped regions (with overdensities  $\delta > 10^4$ ) so the resulting volume filling factor is rather small ( $\sim 10^{-16}$ ). At later times, particles are ejected from these dense regions and their densities rapidly decrease, which results in an increase of  $f_V$ . In this regime, low-density particles, which experienced mechanical (winds) and chemical (metal pollution) feedback from stellar evolution, are dominating. Interestingly, the discrimination by  $Z_{\text{crit}}$  shows a higher filling factor for the particles with  $0 < Z < Z_{\text{crit}}$ , at redshift  $\sim 14$ – $16$ , and a behaviour dominated by the  $Z \geq Z_{\text{crit}}$  – particles, at  $z \lesssim 14$ . This has to be interpreted as a consequence of the metal-enrichment process, as most of the enriched regions enter the PopII regime very rapidly, while the residual PopIII areas are confined to isolated regions or on the border of PopII star-forming sites and contribute less to  $f_V$ . The exact value of the critical metallicity,  $Z_{\text{crit}}$ , does not alter significantly the properties of metal pollution, because of the high metal yields of early stars: larger  $Z_{\text{crit}}$  slightly postpone the epoch when PopII becomes dominant, while smaller  $Z_{\text{crit}}$  anticipate it. In the extreme case of  $Z_{\text{crit}} = 10^{-6} Z_\odot$ , then,  $f_V$  is immediately led by the PopII regime, basically since the onset of star formation. A Salpeter-like PopIII IMF will only induce a short delay in the overall behaviour, due to the longer stellar lifetimes (see also Maio et al. 2010). To illustrate the insensitivity of the volume filling factor to the adopted value of  $Z_{\text{crit}}$ , in the same Fig. 1 (right-hand panel) we compare the filling factors obtained for simulations having different critical metallicities: dotted, solid, dashed, dot-dashed lines refer to  $Z_{\text{crit}} = 10^{-3} Z_\odot$ ,  $Z_{\text{crit}} = 10^{-4} Z_\odot$ ,  $Z_{\text{crit}} = 10^{-5} Z_\odot$  and  $Z_{\text{crit}} = 10^{-6} Z_\odot$ , respectively. As expected, there are no strong variations among these cases, and despite some differences at the initial times, the overall trends easily converge. The one order of magnitude difference in the very early epoch is a consequence of the chemical feedback: higher values of  $Z_{\text{crit}}$  allow the PopIII regime to last longer and to pollute more with respect to the lower  $Z_{\text{crit}}$  cases.

### 3.2 Statistics

To go deeper into the analysis, we study in detail the relevant statistical properties of the gas during the early stages of metal enrichment, and then we show the implications for the PopIII and PopII regimes.

#### 3.2.1 Global features

In Fig. 2, we show the redshift evolution of metal-enriched particles in the phase diagram ( $\rho$ – $T$ ), at  $z = 15.00$  (left),  $z = 13.01$  (centre) and  $z = 11.00$  (right). The colour scale denotes the fraction of particles at any given density and temperature. The corresponding age of the Universe is  $2.66 \times 10^8$ ,  $3.24 \times 10^8$  and  $4.09 \times 10^8$  yr. In the plots, we immediately recognize the gas which falls in the haloes and gets shock heated (low densities and low temperatures), the isothermal phase (where the heating is counterbalanced by cooling, resulting in a roughly constant temperature of  $\sim 10^4$  K), and the catastrophic cooling branch of overdense gas (high densities and low temperatures) that enters the star-forming regime as soon as it reaches a threshold of  $\sim 140 h^2 \text{ cm}^{-3}$ . Above this threshold, stochastic star formation and feedback effects take place (high density and high temperatures) and lead the hot outflows from dense environments into lower density regions (low densities and high temperatures). What emerges from the diagrams is also the behaviour of metal enrichment after the initial pollution events. At the beginning (left-hand panel), only the gas at high number densities ( $\sim 10^2$ – $10^3 h^2 \text{ cm}^{-3}$ ) is affected, as this is where star formation is occurring. As star formation and metal spreading proceed, the surrounding, lower density regions are the next to be affected by metal pollution. The high-temperature particles ( $T > 10^4$  K in the diagrams) are the ones impacted by SN feedback: in particular, hot, dense gas has been heated, within star-forming regions, by the high SN temperatures (thermal feedback), while hot, low-density gas has been ejected from star-forming regions by SN winds (wind feedback). Interestingly, the enrichment pattern of the phase diagram follows the molecular catastrophic-cooling branch, meaning that an ‘inside-out’ pollution mode is taking place. Indeed, since the critical density, in the  $\Lambda$ CDM model, at  $z \sim 11$ , is roughly  $10^{-26} h^2 \text{ g cm}^{-3}$ , Fig. 2 suggests that the very early enrichment process affects the

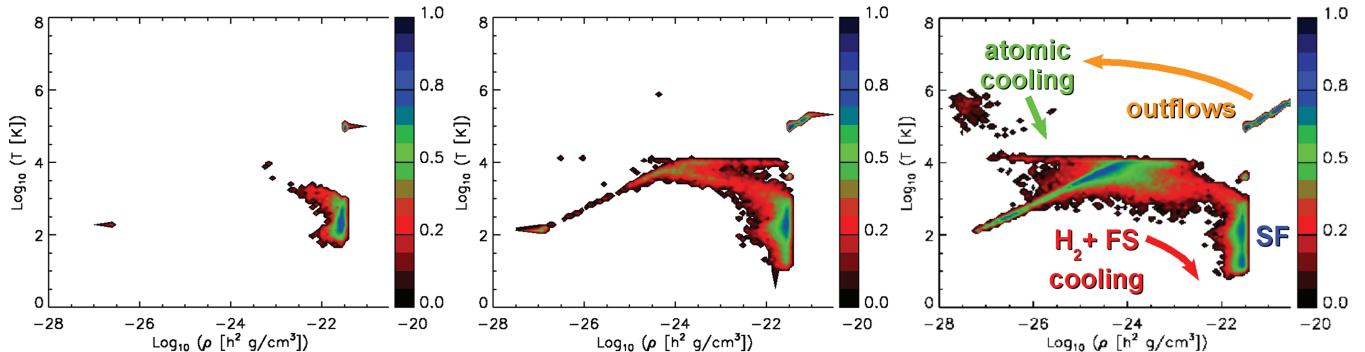


**Figure 2.** Redshift evolution of metal-enriched particles in the  $\rho$ – $T$  diagram. Data refer to redshift  $z = 15.00$  (left),  $z = 13.01$  (centre), and  $z = 11.00$  (right). The colour scale corresponds to the fraction of particles in a given pixel (normalized to 1). The critical density at  $z = 11$ , in the standard  $\Lambda$ CDM model, corresponds to  $\sim 10^{-26} h^2 \text{ g cm}^{-3}$ . In the right-hand panel, mechanical and thermodynamical evolution of the gas is shown at different stages, via different arrows (see labels): low-temperature cooling from molecules (mainly  $\text{H}_2$ ) or fine-structure transitions leads to star formation and subsequent gas outflows into the low-density regions; there hot gas cools down to  $\sim 10^4$  K via resonant atomic transitions and below  $10^4$  K via molecular and fine-structure transitions.

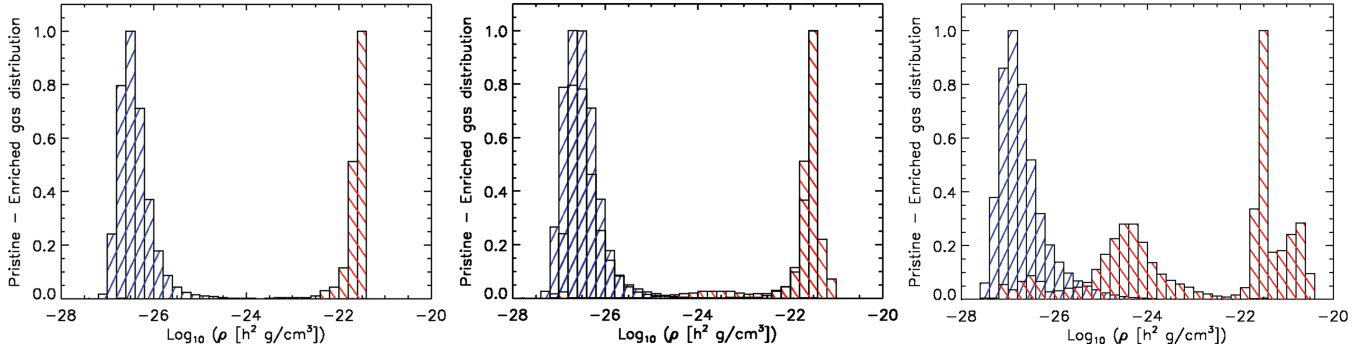


**Figure 3.** Redshift evolution of gas density distribution. Data refers to redshift  $z = 15.00$  (left),  $z = 13.01$  (centre) and  $z = 11.00$  (right). The histograms filled by  $45^\circ$  blue lines refer to pristine gas, while the ones by  $135^\circ$  red lines to enriched gas. Normalization is fixed to 1 for the maximum, in both cases.

collapsed objects<sup>4</sup> by moving from the centre towards the borders and the lower density environments.

Correspondingly, in Fig. 3, we show the gas distribution (histograms) at redshift  $z = 15.00$  (left-hand panel),  $z = 13.01$  (central panel) and  $z = 11.00$  (right-hand panel). The histograms filled by red  $135^\circ$  lines refer to enriched gas, and the ones with blue  $45^\circ$  lines to pristine gas. Most of the particles at low densities are pristine, while the peak of the distribution for metal-enriched gas is at high density, where most of the metals are being produced: these ‘hybrid’ particles are the ones where the subgrid modelling of the multiphase medium and star formation is being applied. As time passes, metal spreading produces a split, with a second peak at lower and intermediate densities. This second peak represents the isothermal stage before the run-away collapse. Its location is very meaningful, since it gives us some idea of the environment affected by metal pollution. The reason for the aggregation of enriched particles in this stage of the phase diagram is due to the long cooling time-scales at low density, in comparison to the cooling branch. Particles that underwent star formation process are spread around from wind feedback. They are hot ( $T \sim 10^5$ – $10^6$  K) and are ejected into lower density regions, where their cooling capabilities allow the temperature to rapidly drop down to  $T \sim 10^4$  K. Subsequent cooling is slightly slower (as observable from the larger spread below  $\sim 10^4$  K, in Fig. 2), due to the less efficient metal fine-structure transitions, but it still dominates the total cooling function, with respect to the molecular contribution. The lack of particles in correspondence of high/intermediate densities and high temperatures is due to the feedback effects combined with strong cooling, which allow the gas to easily cool down to  $T \lesssim 10^4$  K. Indeed, due to feedback from SN, entropy is injected into the star-forming medium and the gas is pushed away towards low-density areas. The typical velocity for stellar winds is  $500 \text{ km s}^{-1}$ , thus in  $\sim 10^6$ – $10^7$  yr the gas can be pushed several kpc away,<sup>5</sup> beyond the isothermal peak (see Fig. 2), where densities are orders of magnitude smaller.

By comparing the distribution at different redshifts, it turns out that the mass fraction of enriched material located in overdense [i.e. selected with overdensity  $\delta \equiv \rho/\rho_{\text{cr}}(z) \gtrsim 10^2$ ] regions is still more than  $\sim 99$  per cent at  $z \sim 13$ , and decreases down to  $\sim 87$  per cent at

$z \sim 11$ , i.e.  $\Delta t \sim 0.08$  Gyr later. At this redshift, the fraction of new metals,  $f_{Z,\text{new}}$ , represents more than 90 per cent, and the corresponding enrichment rate,  $\dot{\varepsilon}_Z \equiv d f_Z/dt \simeq f_{Z,\text{new}}/\Delta t$ , is  $\sim 10^{-8} \text{ yr}^{-1}$ . When looking at the amount of metals moving along the cooling branch,<sup>6</sup> we find that  $\sim 1$ ,  $\sim 6$  and  $\sim 4$  per cent of the enriched mass at redshift  $z = 15.00$ ,  $13.01$  and  $11.00$ , respectively, is undergoing run-away collapse.

Comparison of the simulations with different  $Z_{\text{crit}}$  shows that this picture does not change dramatically, and the enriched mass undergoing run-away cooling increases, in all the cases, up to around 5–7 per cent at  $z = 13.01$ , and reaches about 3–6 per cent at  $z = 11.00$ .

If we look at the run with a Salpeter-like PopIII IMF (see details in Maio et al. 2010, in particular fig. 7), stellar lifetimes are longer, and consequently also the time-delay for metal spreading is longer ( $\sim 10^7$  yr). So, metal-rich particles undergoing run-away cooling are significantly present only after  $z \lesssim 14$  and account for  $\sim 3$ – $8$  per cent of the enriched mass.

In Fig. 4, we investigate how gas mass metallicity correlates with overdensity. We consider metal-enriched particles and compute the joint probability distribution between  $Z$  and  $\delta$ ,  $P(\delta, Z)$ , and the conditional probability distributions,  $P(\delta|Z)$ , and  $P(Z|\delta)$ . The joint probability distribution,  $P(\delta, Z)$ , is computed by summing up all the metal contributions at any  $\delta$  and  $Z$  and normalized over the whole  $\{\delta, Z\}$  space. While the conditional probability  $P(Z|\delta)$  is computed by summing up all the contributions for a given  $\delta$ , and normalized over the corresponding  $\{Z\}$  subspace. Similarly, the conditional probability  $P(\delta|Z)$  is computed by summing up all the contributions for a given  $Z$ , and normalized over the corresponding  $\{\delta\}$  subspace. The horizontal line marks the critical value,  $Z_{\text{crit}}$ , while the vertical line marks the star formation density threshold ( $\sim 140 h^2 \text{ cm}^{-3}$ ), above which the star formation subgrid modelling is applied. The plots refer to redshift  $z = 11$  (upper row),  $z = 13$  (central row) and  $z = 15$  (bottom row). The joint probability distribution,  $P(\delta, Z)$ , has a maximum around  $Z \sim 10^{-6}$ – $10^{-4}$ , almost despite of the redshift considered, and its time evolution shows clearly how metals are ejected by wind feedback from the star-forming regions, at  $\delta \sim 10^4$ – $10^5$ , to the lower density ones, at  $\delta \lesssim 10^2$ . This process is better highlighted in the conditional probability distribution  $P(Z|\delta)$ : at earlier times, during the very first episodes of star formation, there

<sup>4</sup> According to the ‘top-hat’ model, collapsed objects are the ones with densities of the order of  $\sim 200$  times the critical one.

<sup>5</sup> The physical distance travelled at  $500 \text{ km s}^{-1}$  in  $10^6$ – $10^7$  yr is  $\sim 0.5$ – $5$  kpc, corresponding to  $\sim 8$ – $80$  kpc comoving, at redshift 15.

<sup>6</sup> The cooling branch roughly corresponds to densities higher than  $\sim 10^2$  times the critical one and below the star formation threshold of about  $140 h^2 \text{ cm}^{-3} \sim 10^{-22} h^2 \text{ g cm}^{-3}$ .

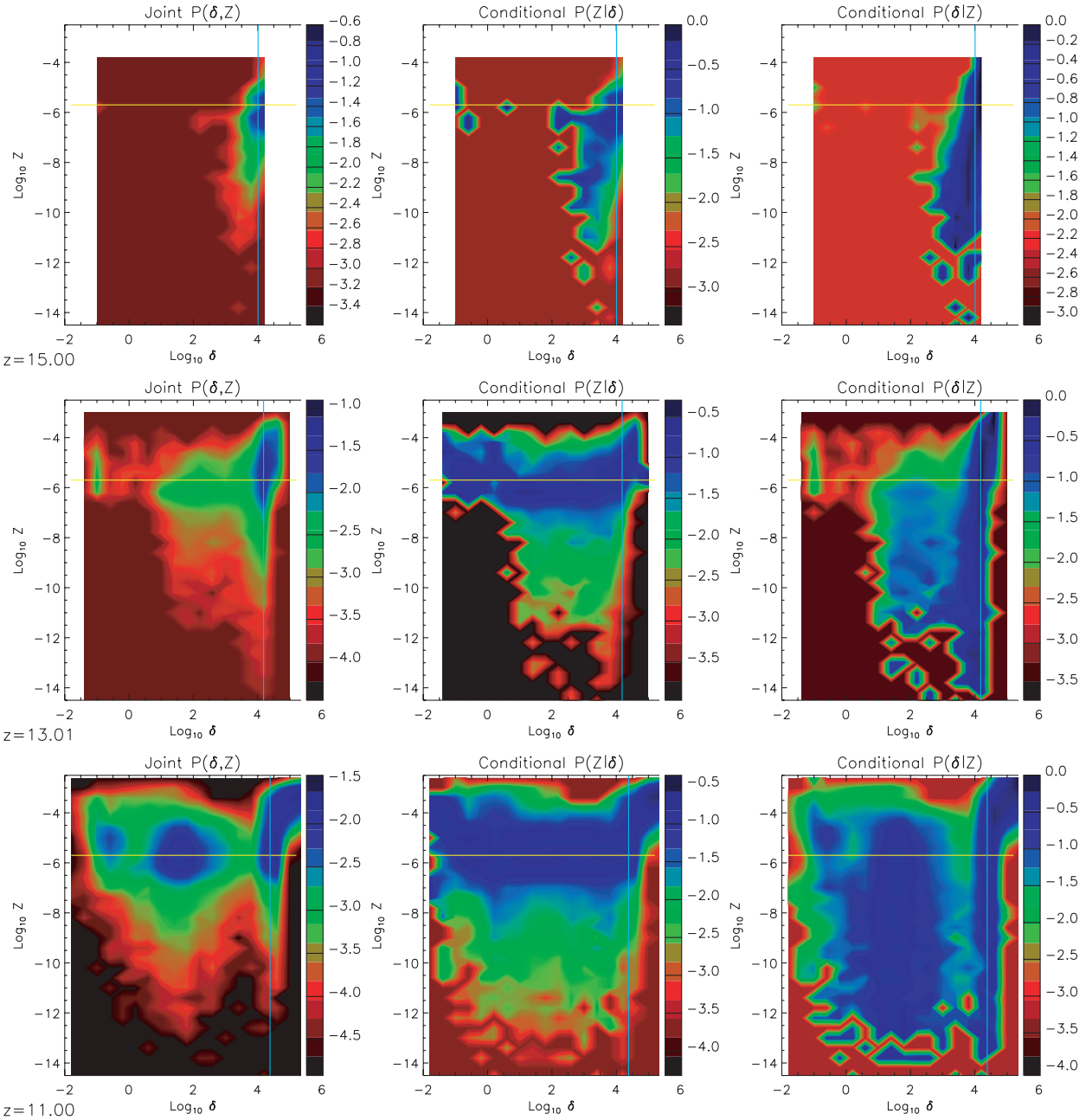


**Figure 4.** Normalized joint probability distribution (left column),  $P(\delta, Z)$ , between metallicity,  $Z$ , and overdensity,  $\delta$ , at redshift  $z = 15.00$  (top),  $z = 13.01$  (centre) and  $z = 11.00$  (bottom). The corresponding conditional probability distributions,  $P(Z|\delta)$  and  $P(\delta|Z)$ , are also shown in the central and right column, respectively. In each panel, the horizontal, solid line is drawn in correspondence of the critical metallicity,  $Z_{\text{crit}} = 10^{-4} Z_{\odot}$  and the vertical, solid line marks the star formation overdensity threshold.

are still few metals, mostly at low  $Z$ , and they have not reached yet the low-density environments. Later on,  $P(Z|\delta)$  is rapidly boosted to higher metallicities, with  $Z$  overcoming  $Z_{\text{crit}}$  at any  $\delta$ , as a consequence of the high metal yields of primordial stars. By checking the conditional probability  $P(\delta|Z)$ , it emerges that, for any fixed  $Z$  besides the star-forming particles at  $\delta \sim 10^4$ – $10^5$ , the regions where enrichment due to metal-spreading is dominant are soon the ones with  $\delta \lesssim 10^2$  (see also previous sections). Furthermore, the overdensity range between  $\sim 10^2$  and  $\sim 10^4$ , at  $z \sim 11$ , presents a gap in the distribution, because it corresponds to the fast, catastrophic run-away cooling, through which enriched gas rapidly recollapses to higher densities and lower temperatures.

### 3.2.2 PopIII and PopII

After our investigation of the global features of the primordial enrichment, we want to study the differences between PopIII and PopII regimes.

In Fig. 5, we select particles according to their metallicity and plot the density distribution of metal-rich particles for both PopII and PopIII ones (in a similar way to Fig. 3). By comparing the distributions of particles that have  $Z \geq Z_{\text{crit}}$  (first row) and  $Z < Z_{\text{crit}}$  (second row), it is easily shown that, in both cases, enriched star-forming particles are continuously produced by the ongoing star formation, and, while the Universe evolves, wind feedback pushes

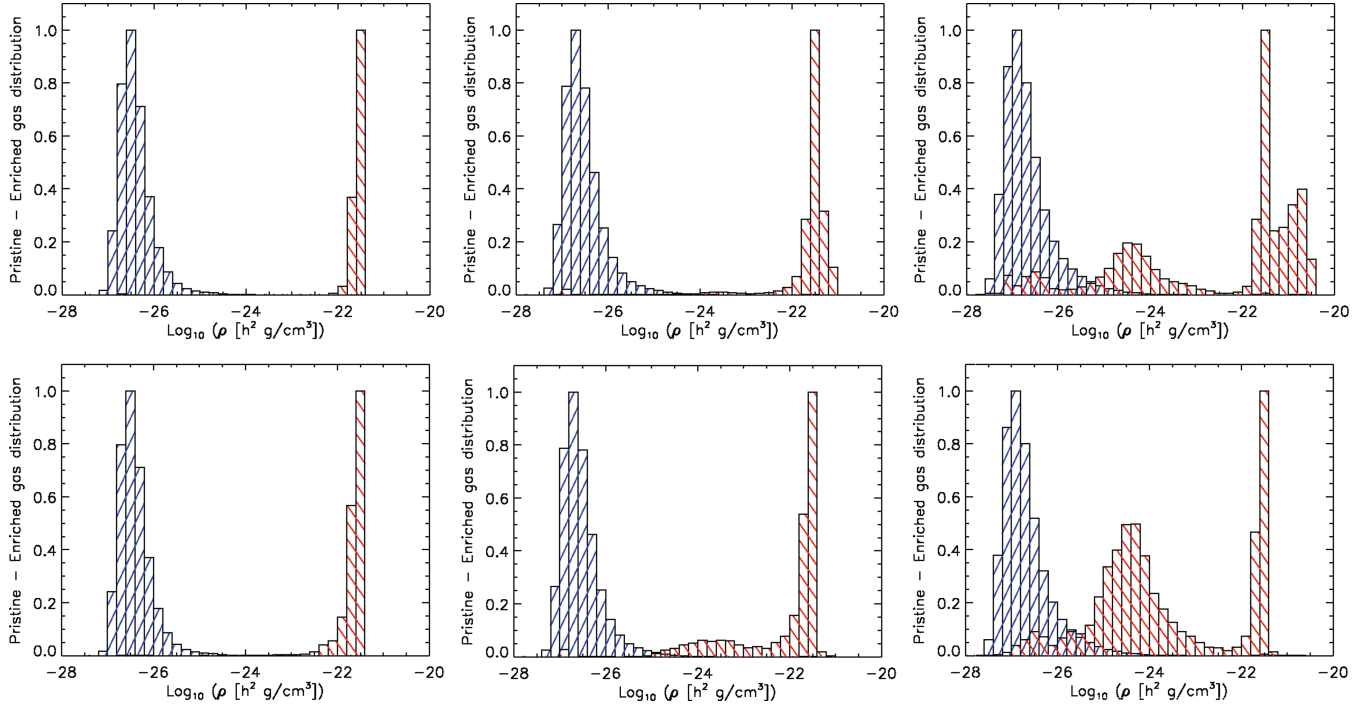


**Figure 5.** Redshift evolution of gas density distributions of pristine and metal-rich particles, selected by their  $Z$ . In both rows, we show the pristine-gas distribution with histograms filled by  $45^\circ$  blue lines, while enriched gas distributions, for particles having  $Z \geq Z_{\text{crit}}$  in the upper row and  $Z < Z_{\text{crit}}$  in the lower row, are plotted with histograms filled by  $135^\circ$  red lines. Data refer to  $z = 15.00$  (left),  $z = 13.01$  (centre) and  $z = 11.00$  (right). Normalization is fixed to 1 for the maximum.

**Table 1.** Mass fractions of enriched gas.

Redshift	PopII relative fraction	PopIII relative fraction
15	43 per cent	57 per cent
13	94 per cent	6 per cent
11	99 per cent	1 per cent

them towards external, lower density regions (see Tornatore et al. 2007b). In particular, the relative fraction of PopIII particles outside the collapsed objects is more than a factor of 2 higher than the PopII one. Let us discuss these two cases more in detail (see also Table 1).

(i) *PopII*. The mass fraction of metals with  $Z \geq Z_{\text{crit}}$  is initially zero, but reaches already  $\sim 43$  per cent at  $z \sim 15$  and rapidly rises up to  $\sim 94$ – $99$  per cent at  $z \sim 13$ – $11$ , and above at later times. The polluted material is pushed away from the overdense regions and expands with time. In particular, about  $\sim 23$  per cent of formed PopII material has travelled into surrounding  $\delta < 10^2$  regions, by redshift  $z \sim 11$  – a time lag of  $\sim 2 \times 10^8$  yr.

(ii) *PopIII*. For the very low metallicity particles, the picture is quantitatively quite different and particles with  $Z < Z_{\text{crit}}$  are found outside the collapsing regions, in a more significant way. The onset of star formation is initially dominated by PopIII, but shortly after, at  $z \sim 15$ , the residual enriched mass fraction with  $Z < Z_{\text{crit}}$  drops down  $\sim 57$  per cent, and becomes just  $\sim 6$  per cent at  $z \sim 13$ , and  $\sim 1$  per cent at  $z \sim 11$ .

Let us now focus on the properties of the enriched cooling mass only (see Table 2), i.e. the mass which has experienced wind feedback and is cooling back into star-forming sites. In the initial stages, as mentioned in Section 3.2, roughly  $\sim 1$  per cent of the enriched

**Table 2.** Mass fractions of the enriched cooling gas.

Redshift	PopII cooling relative fraction	PopIII cooling relative fraction
15	3 per cent	97 per cent
13	80 per cent	20 per cent
11	94 per cent	6 per cent

mass is in the catastrophic cooling regime, and this fraction slightly increases up to 4–6 per cent at  $z \sim 11$ . At  $z \sim 15$ , the enriched cooling mass is made of PopIII type for  $\sim 97$  per cent and of PopII for  $\sim 3$  per cent. After that, the situation completely changes and, at  $z \sim 13$ , the PopIII part is only  $\sim 20$  per cent, and the PopII rapidly increases up to  $\sim 80$  per cent. Later on, at  $z \sim 11$ , the residual PopIII mass fraction drops down to  $\sim 6$  per cent and the PopII one increases up to  $\sim 94$  per cent. At lower redshifts, the PopIII part becomes negligible with respect to the PopII one. Also in this case, different values for  $Z_{\text{crit}}$  do not induce drastic changes: the PopIII material is significantly present only at the very first stages and completely replaced by PopII at  $z \lesssim 14$ – $13$ , although occurs more quickly for lower  $Z_{\text{crit}}$ .

When a Salpeter-like PopIII IMF is adopted, the residual collapsing PopIII material at  $z \lesssim 14$  is again only a few per cent (more precisely,  $\sim 3$  per cent at  $z \sim 11$ ).

### 3.3 Dynamics

To get a better understanding of metal pollution at early times, we discuss the dynamical features of the material involved in the spreading process. As an example, we focus on the evolution of the most massive dark-matter halo (mass between  $\sim 10^7$  and  $10^8 M_\odot h^{-1}$  at

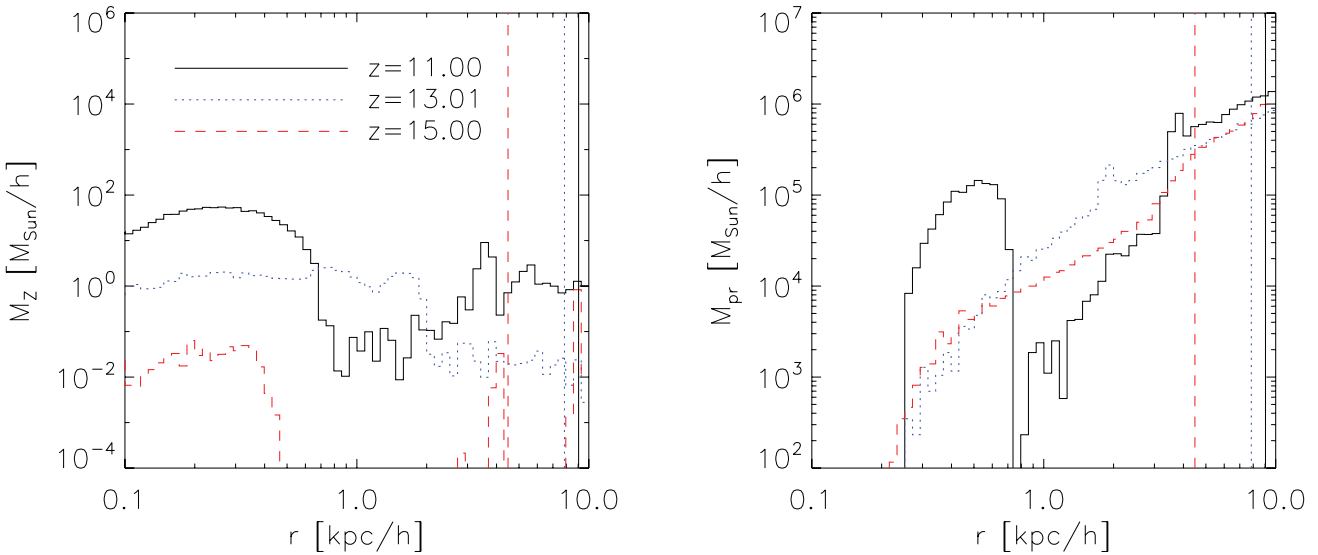


**Figure 6.** Mass profiles as a function of comoving radius for enriched (left-hand panel) and pristine (right-hand panel) gas at redshift  $z = 11.00$  (solid lines),  $z = 13.01$  (dotted lines) and  $z = 15.00$  (dashed lines). Each vertical line corresponds to the virial radius at each redshift. The comoving gas softening length is  $\sim 0.1 \text{ kpc } h^{-1}$  and the minimum gas smoothing length is  $\sim 0.14 \text{ kpc } h^{-1}$ .

$z \sim 16\text{--}10$ ) and compute radially averaged quantities. The comoving virial radius is computed as the distance from the centre of mass at which the average enclosed overdensity is  $\sim 200$ , and, at these stages, it varies between  $\sim 4$  and  $9 \text{ kpc } h^{-1}$ . We note that such overdensities include the whole cooling branch and a relevant part of the isothermal gas phase (see e.g. Fig. 2).

### 3.3.1 Global features

In Fig. 6, we show the mass profiles for metal-enriched and pristine gas of the main halo, at different redshift. The vertical lines refer to the virial radius at each redshift. Pollution starts at  $z \sim 16$ , when the early PISN spread the first metals. From this moment on, star formation contributes more and more to metal spreading and the ‘inside-out’ mode of metal enrichment is visible in the time sequence shown throughout the panels, as more and more surrounding regions are affected by pollution. The structure of the pristine gas seems strongly influenced by star formation and feedback effects. In fact, while star formation goes on and the metallicity of the environment increases, the pristine gas is always kept at  $\sim 0.2 \text{ kpc}$  (comoving): early PopIII activity halts it from getting accumulated towards the centre. Only at redshift  $z \lesssim 13$ , when the residual PopIII contribution to the SFR is just  $\sim 10^{-3}$ , the PopII regime dominates, the infall becomes more efficient and this determines the bump at small radii. The average amount of metal mass in the shells is some orders of magnitude lower than the pristine gas, but locally, it is possible to find highly enriched areas with metallicities up to  $Z \sim 10^{-3}$ , i.e.  $\sim 10^{-1} Z_\odot$  (e.g. see at radii of  $\sim 0.3 \text{ kpc } h^{-1}$ , in Fig. 6). Winds are also able to spread around material beyond the virial radius, into nearby empty regions.

This behaviour is confirmed in Fig. 7, where we show corresponding mass inflow and outflow rates for metal-rich and pristine gas, in the main halo. These are computed as

$$\frac{dM}{dt} \simeq \frac{\Delta M}{\Delta r} v_{\text{rad}}, \quad (2)$$

with  $\Delta M$  mass,  $\Delta r$  the radial bin and  $v_{\text{rad}}$  average radial velocity for the considered shell. The pristine-gas infall rate is  $\sim 10^{-3}\text{--}$

$10^{-1} M_\odot \text{ yr}^{-1}$ . The metal outflow rates are a few orders of magnitude lower than the infalling rates of pristine gas, but the continuous ejection of metals from PISN/SN pollutes the surroundings up to distances exceeding the virial radius. This is recovered in the inflow rates of the enriched gas. While the innermost regions are dominated by chaotic turbulent motions (see following discussion), the outermost enriched mass, situated at distances comparable with the virial radius, is definitely decoupled from the metals in the core and is fastly moving inwards (the radial component of the velocity easily reaches  $\sim 50 \text{ km s}^{-1}$ ). This incoming material has just been pushed away from other sources and undergone wind feedback. It gets into the main halo already at  $\sim 16$ , and, in the following stages, polluted material systematically replenishes the innermost regions. Its contribution to the mass profiles becomes comparable or even dominant from  $\sim 0.5 \text{ kpc } h^{-1}$  (comoving) up to larger radii. Since wind feedback is the main responsible for metal spreading up to distances larger than a few  $\sim \text{kpc}$  within  $\sim 10^7 \text{ yr}$ , the presence of metals in these dense environments after very short time-scales is a striking sign of pollution from nearby star-forming haloes, whose particles are ejected and trapped in the neighbouring collapsed regions. The whole process, thus, leads to the concept of ‘gravitational enrichment’, i.e. metal enrichment induced by different, external sources, whose polluted material is expelled and recaptured by the gravitational field of closeby haloes, located at some  $\text{kpc}$  away. This reminds of genetic enrichment (e.g. Scannapieco, Schneider & Ferrara 2003), but, in this case, there is no obvious parental relationship (child/progenitor haloes) among the involved objects and they can have quite distinct evolution history. In contrast to self-enrichment, that is probably the main way of enriching rare, isolated haloes, up to overcritical  $Z$ , the gravitational-enrichment mechanism appears to be the dominant one, especially in crowded and actively star-forming environments: it can highly boost the metallicities and allow the gas to exceed  $Z_{\text{crit}}$  in only  $\sim 10^7 \text{ yr}$  (see further discussion in Section 4).

In Fig. 8, we show velocity maps for enriched and pristine gas, at different redshifts. The initial collapse of primordial gas appears along the field lines at high  $z$  (left column). This leads to star formation, followed by metal pollution, with consequent spreading of

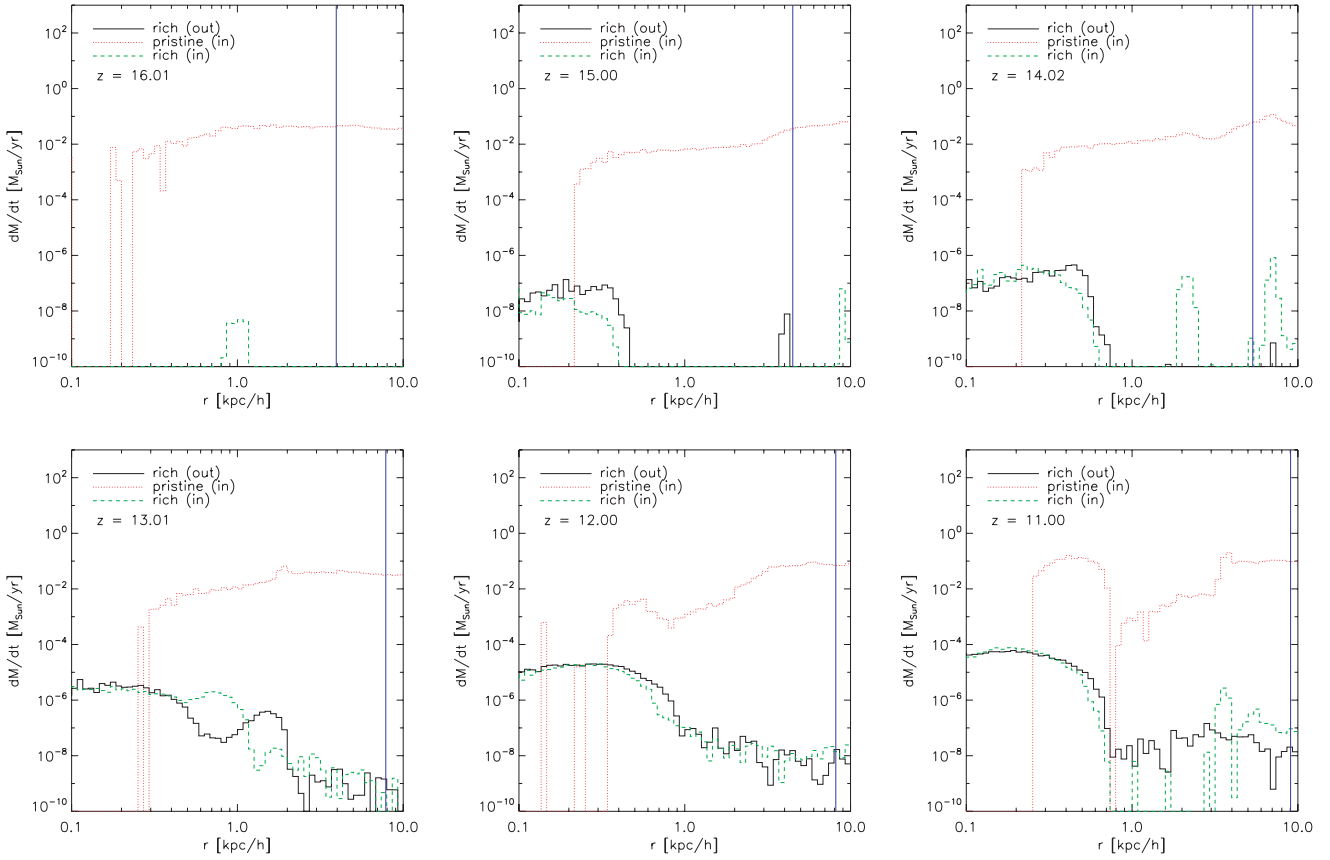


**Figure 7.** Mass outflow rates for enriched gas (solid lines), and inflow rates for both pristine gas (dotted lines) and enriched gas (dashed lines). Redshifts are  $z = 16.01$  (upper left),  $z = 15.00$  (upper centre),  $z = 14.02$  (upper right),  $z = 13.01$  (lower left),  $z = 12.00$  (lower centre) and  $z = 11.00$  (lower right). The vertical lines are the corresponding virial radii.

particles, because of wind effects. Since the typical temperatures of the star-forming regions vary between a few hundred kelvin (for the cold phase) and  $\sim 10^6$  K (for the gas heated by SN feedback), the local sound speed is  $\sim 1-10^2 \text{ km s}^{-1}$ , and, therefore, the star-forming environment is characterized by supersonic flows. Moreover, the interplay between the hot, outflowing, enriched gas (central and right column) and the cold, infalling, pristine gas leads to the development of a turbulent regime on kpc scales. To quantify this,<sup>7</sup> we give an order-of-magnitude estimate of the Reynolds number (e.g. see Elmegreen & Scalo 2004, and references therein),

$$R \sim ul/\nu \sim \mathcal{M} l n \sigma, \quad (3)$$

with,  $u$  velocity,  $l$  typical scale of the flux,  $\nu$  kinematic viscosity of the gas,  $\mathcal{M}$  Mach number,  $n$  number density and  $\sigma$  particle cross-section. We have  $u \sim 10^2 \text{ km s}^{-1}$ , a fiducial scale – see Figs 6 and 7 – of  $l \sim \text{kpc}$  (in the simulations the typical dimensions of the star-forming regions at the redshifts of interest go up to several comoving kpc), and  $\nu \sim c/n\sigma$ , where  $c$  is the sound speed. Typical densities of the star-forming regions are  $n \gtrsim 10^2 \text{ cm}^{-3}$ , with  $\sigma \sim 10^{-15} \text{ cm}^2$  (Elmegreen & Scalo 2004). This implies  $\nu \sim 10^{18}-10^{20} \text{ cm}^2 \text{ s}^{-1}$ , and  $R \sim 10^8-10^{10}$ . Such high Reynolds numbers arise from the strongly turbulent state of the star-forming regions. These are, of course, order-of-magnitude estimates, but they are solid enough to

characterize the nature of such flows. In addition, the interactions between different gas phases generate strong hydro-instabilities: e.g. Raleigh–Taylor instabilities, originated by the hot, enriched gas pushing against the cold, pristine one in its surroundings (shocks), or Kelvin–Helmholtz instabilities, due to the velocity differences between the outgoing, enriched gas and the infalling, pristine gas. The interplay among the two phases is very evident in the pristine-gas field lines (left column), compared with the simultaneous metal-gas ones (central column), and with the corresponding velocity maps (right column). These considerations are expected to hold not only in this particular case, but also for other small primordial haloes, that are highly affected by feedback effects.

### 3.3.2 PopIII and PopII

In Fig. 9, we summarize our findings about chemical feedback by showing in detail the radial distribution of PopIII and PopII species, in the innermost regions of the main halo, at redshift 15.00, 13.01 and 11.00. As time passes, the most striking and evident feature is the gradual disappearance of the PopIII generation. At  $z \sim 15$ , almost half of the gas is still PopIII at comoving distances  $\gtrsim 0.2 \text{ kpc } h^{-1}$ . Later on, at  $z \sim 13$ , the situation is similar, but the residual PopIII gas is found at larger and larger distances from the centre (more than  $\sim 2 \text{ kpc } h^{-1}$  comoving). Indeed, new polluted material has been ejected, and, as a consequence, the metallicities of the pre-enriched regions have increased. So, only the pristine gas far away from star formation sites can maintain a residual metallicity

<sup>7</sup> The effects of numerical viscosity on structure masses and velocity fields are widely discussed in literature. See e.g. Dolag et al. (2005), Valdarnini (2011) or appendix A in Biffi, Dolag & Boehringer (2011).

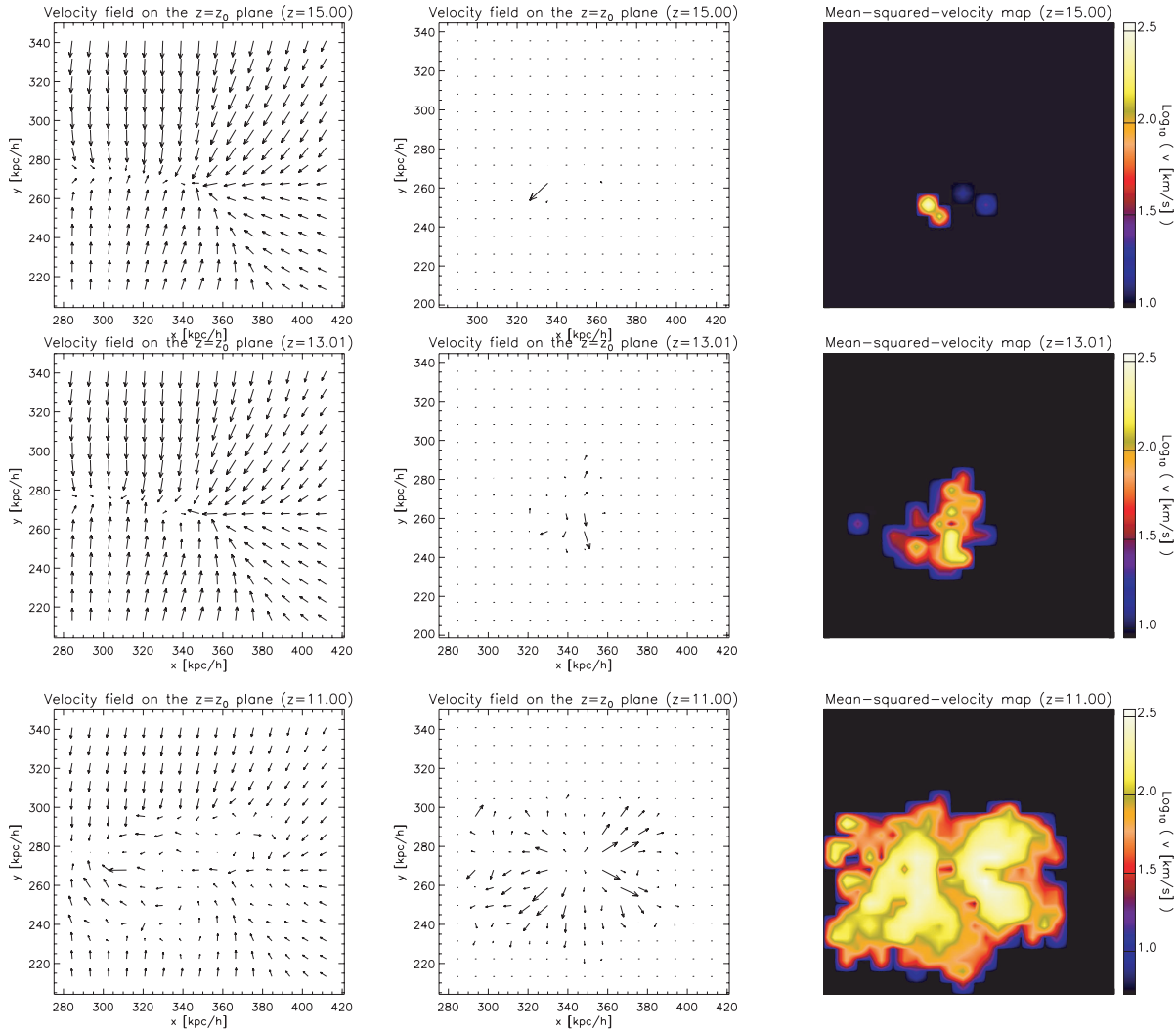


**Figure 8.** Redshift evolution of the velocity field lines for pristine gas (left column), and metal-rich gas (central column). Corresponding mean-squared velocity maps for metal-rich gas are shown on the right column. The selected region is a zoom-in on the plane  $z = z_0 \simeq 370 \mathrm{~kpc} h^{-1}$  (comoving) of the main star-forming halo.

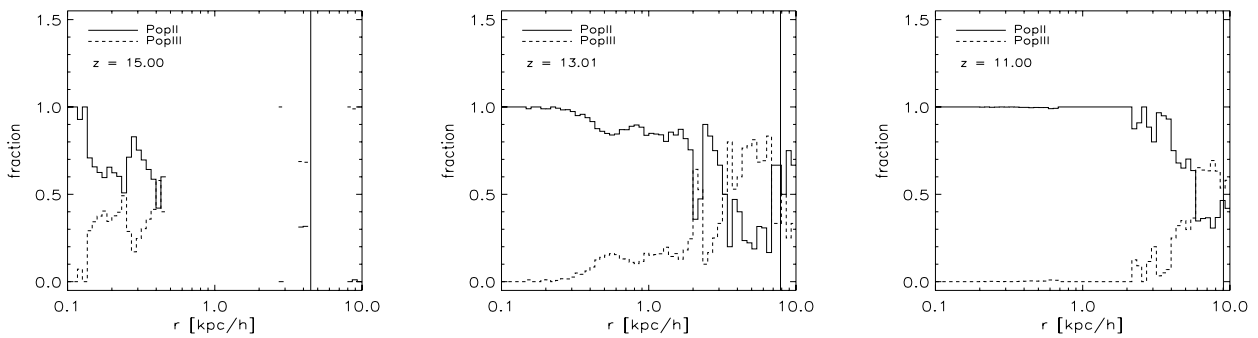


**Figure 9.** Average fractions of PopII (solid lines) and PopIII (dashed lines) species as a function of comoving radius for the enriched material. The vertical lines indicate the virial radius. Data refer to  $z = 15.00$  (left),  $z = 13.01$  (centre) and  $z = 11.00$  (right).

below  $Z_{\mathrm{crit}}$ . By redshift  $\sim 11$ , ongoing spreading events will continue to confine the pristine gas to the peripheral regions, several kpc away from the centre. Very similar trends are found when considering separately the infalling portion and the outflowing portion of the gas.

#### 4 DISCUSSION AND CONCLUSIONS

We summarize, now, how, throughout this paper, we have addressed the issues presented in the introduction (Section 1). We have studied early structure formation and metal pollution by analysing

numerical *N*-body/SPH simulations, as described in Maio et al. (2010). With respect to other implementations of metal spreading present in literature (e.g. Raiteri, Villata & Navarro 1996; Gnedin 1998; Mosconi et al. 2001; Lia, Portinari & Carraro 2002a, 2002b; Kawata & Gibson 2003; Kobayashi 2004; Ricotti & Ostriker 2004; Scannapieco et al. 2005; Tornatore et al. 2007a; Oppenheimer et al. 2010; Finlator, Oppenheimer & Davé 2011), our implementation additionally follows proper molecular-chemistry treatment of  $e^-$ , H,  $H^+$ ,  $H^-$ , He,  $He^+$ ,  $He^{++}$ ,  $H_2$ ,  $H_2^+$ , D,  $D^+$ , HD and  $HeH^+$ ; the evolution of individual metal species (C, O, Mg, S, Si and Fe, since they are the most abundant element produced during stellar evolution); the transition from the early PopIII regime to the subsequent PopII regime and stellar feedback for star-forming particles.

Metal enrichment takes place efficiently with run-away molecular cooling leading to the first PopIII star formation events, and to the following, rapid transition to PopII. As a consequence of the chemical feedback, higher values of  $Z_{\text{crit}}$  allow the PopIII regime to last a bit longer (at most  $<8 \times 10^7$  yr) and to pollute more with respect to the lower  $Z_{\text{crit}}$  cases (Maio et al. 2010). The first sites of metal pollution are clumped and dense star-forming regions from which metals are spread away via feedback effects.

Because of this process starting in regions with overdensities higher than  $\delta \sim 10^4$ , the metal filling factor (Section 3.1) is extremely small at initial times, and subsequently increases by several orders of magnitude, when metals get into lower density and larger volume regions (see Fig. 1, left-hand panel). In roughly  $2 \times 10^8$  yr, there is a steep increment of about 8 orders of magnitude, due to the explosions of the early, short-lived, massive stars and the pollution of low-density regions. Discrimination by  $Z_{\text{crit}}$  allows us to see that PopIII particles dominates the filling factors only at high redshift, and are expected to be found in less dense or more isolated regions at later times. The precise value of  $Z_{\text{crit}}$  in the range  $[10^{-6}, 10^{-3}] Z_\odot$  seems to be not crucial for the properties of primordial gas and metal enrichment (Fig. 1, right-hand panel), as also argued in Maio et al. (2010).

The phase-space evolution (Fig. 2) and the probability distributions (Figs 3 and 4) clearly indicate a dominant ‘inside-out’ mode of metal pollution, according to which metals are strongly spread from the clumped regions to the low-density regions. Within a time of  $\sim 10^8$  yr, the newly enriched material accounts for  $\sim 90$  per cent of the ejected metals (see Section 3.2, where we compute the enrichment rate  $\dot{\varepsilon}_Z \sim 10^{-8}$  yr). Moreover, the fraction of enriched material expelled by the winds that falls in the run-away collapsing region and becomes available again for star formation reaches values of  $\lesssim 10$  per cent (see Section 3.2). Details about the exact value of  $Z_{\text{crit}}$  alter only slightly these findings. In order to see the effects of different PopIII IMFs, we have also compared the top-heavy case with the Salpeter case. In the latter, a slightly longer delay of metal enrichment is found, due to the longer stellar lifetimes, but the subsequent pollution history is quite similar (see also Maio et al. 2010, for more details).

Our dynamical analysis (e.g. Figs 6, 7 and 8) confirms that pristine-gas inflow rates of  $\sim 10^{-3}-10^{-1} M_\odot \text{ yr}^{-1}$  coexist with metal outflows a few orders of magnitude smaller. Metal-rich winds of hundreds  $\text{km s}^{-1}$  are responsible for pollution of the medium even beyond the virial radii, induce hydro-instabilities, and cause turbulence with Reynolds numbers of  $\sim 10^8-10^{10}$  (Section 3.3).

Accumulation of metals in the high-density regions is led by ‘gravitational enrichment’ that can boost the metallicity in a few  $10^7$  yr (see e.g. Figs 6 and 7), without the need to wait for the growth of the halo to re-accrete them (self-enrichment). We note

that alternative scenarios, such as self-enrichment and genetic enrichment, could not explain all the aspects shown by metal pollution at high redshift. For example, due to the high velocity of the material escaping from the star-forming sites, metals can be ejected as far as several kpc away and the halo could effectively re-accrete them only if the growth process were still taking place. Because this requires at least some  $\sim 10^8$  yr (e.g. Greif et al. 2010), self-enrichment would fail in explaining the high metallicities reached in  $\sim 10^7$  yr, as discussed in Section 3.3 (see also Maio et al. 2010). On the other hand, genetic enrichment relies on parental relationships (child/progenitor haloes), and it would not explain metal pollution in haloes which have no direct connections to each other.

More realistically, ‘gravitational enrichment’ can account for the pollution of separate haloes which evolve independently. In fact, when metals are spread beyond the boundaries of a halo (see e.g. previous sections), the gravitational force of a neighbouring halo can attract those metals and accrete them on to it. In this way, metal pollution is enhanced in haloes which have gravitationally trapped metals, originated in completely different environments. The inside-out mode of metal pollution is at the origin of such dynamical behaviour.

Similar results hold for both PopII and PopIII components (see Figs 5 and 9). Due to the previous considerations on metal enrichment, the PopIII material is more likely to be found on the borders of primordial haloes or in isolated, low-density environments ( $\sim 50$  per cent after  $\sim 10^8$  yr), and the PopII one in more clustered regions ( $\sim 87$  per cent after the same time). A few  $10^8$  yr after the onset of star formation, the amount of PopII material becomes highly dominant over the residual PopIII, reaching mass fractions higher than  $\sim 99$  per cent.

One of the most striking conclusions we can draw is related to the rapidity and efficiency by which PopII stars are formed after the first bursts of star formation. Because of the high metal yields of primordial massive PISN/SN and pollution coming from closeby star-forming regions, the transition from the PopIII to the PopII regime is extremely rapid. Moreover, the mass trends presented in the previous sections (see e.g. Figs 6 and 7) support this conclusion, as, due to star formation feedback, inflows do not efficiently replenish the star-forming regions with newly accreted, pristine gas. One can estimate to first order the necessary pristine inflow rates,  $\dot{M}_{\text{prist}}$ , needed to dilute metal-rich gas,  $M_Z$ , to metallicities  $Z < Z_{\text{crit}}$ :

$$\frac{M_Z}{M_Z + \dot{M}_{\text{prist}}} < Z_{\text{crit}}, \quad (4)$$

and

$$\dot{M}_{\text{prist}} > \frac{(1 - Z_{\text{crit}})M_Z}{Z_{\text{crit}}}. \quad (5)$$

That means (for  $Z \ll 1$ ):

$$\frac{\dot{M}_{\text{prist}}}{\dot{M}_Z} > \frac{1 - Z_{\text{crit}}}{Z_{\text{crit}}} \sim \frac{1}{Z_{\text{crit}}}, \quad (6)$$

i.e. for  $Z_{\text{crit}} \sim 10^{-4} Z_\odot$ , one can dilute the ejected metals below  $Z_{\text{crit}}$  only with  $\dot{M}_{\text{prist}}/\dot{M}_Z \gtrsim 5 \times 10^5$ . These huge differences of several orders of magnitude between enriched-gas and pristine-gas rates are usually not reached, as clearly shown in Fig. 7. In general, this is probably what happens in the primordial haloes, which have similar sizes and which experience similar star formation feedback effects.

Furthermore, after the onset of star formation, the hot temperatures induced by SN thermal feedback keep dissociating molecules and it becomes difficult for the pristine gas to cool down: in this

regime, the metal fine-structure transition cooling plays a dominant role, and that is the reason why one finds enriched cooling gas, ejected by wind feedback from nearby sources, deeper in the potential wells. Thus, PopIII can survive mostly outside clumped regions, in isolated, or in low-density environments, where relation (6) is more easily satisfied, while PopII dominates the dense, star-forming environments.

We note that the high resolution of our simulations and the detailed chemistry treatment allow us to make firm, consistent, and robust statements on the gas behaviour, from the pristine, molecular stages, to the following star formation phases, and the PopIII/PopII metal enrichment events. In particular, the simulations include a complete, self-consistent treatment of primordial gas (dealing with cooling and molecule evolution), which is lacking in other simple approximations adopted in several previous works (e.g. Kobayashi 2004; Scannapieco et al. 2005; Tornatore et al. 2007b; Oppenheimer et al. 2010; Finlator et al. 2011). Those implementation can be very useful when investigating metal distributions or present-day star formation, but they obviously fail at high redshift, when molecules are the leading coolants, primordial stars form, and the PopIII/PopII transition takes place. Consistently with those works, metal enrichment is very patchy and inhomogeneous, with a characteristic ‘inside-out’ mode. This is particularly true for the primordial PopIII regime, whose energetics is much more powerful than the PopII one. On the other hand, there are some *caveats*: given the small size of the boxes, we are limited in the statistical sampling of rare, large haloes. In the simulations presented here, there is no radiative-transfer treatment from stars which can affect the very close surroundings of individual massive PopIII stars, by heating and ionizing the gas (e.g. Abel, Norman & Madau 1999; Haiman, Abel & Rees 2000; Ricotti, Gnedin & Shull 2001; Kitayama & Yoshida 2005; Iliev, Shapiro & Raga 2005; Ahn & Shapiro 2007; Wise & Abel 2008; Greif et al. 2009), but for low-mass SN, this effect would be less severe (e.g. Hasegawa, Umemura & Susa 2009; Whalen, Hueckstaedt & McConkie 2010). The inclusion of radiative transfer is relatively easy, though, only when dealing with individual or a few sources. It becomes very problematic and computationally expensive when studying cosmological evolution with enormous numbers of stars whose radiation has to be followed simultaneously with gas chemistry and hydrodynamics. However, we do not expect substantial changes on our overall conclusions about the general picture of the PopIII/PopII transition, or the dynamics of the metals. Indeed, metals ejected with velocities of  $\sim 10^2 \text{ km s}^{-1}$  would probably be very little affected by radiative pressure (e.g. Johnson et al. 2011). The stellar radiation would probably enhance (see e.g. Fig. 6) the evacuation of pristine gas from the individual minihaloes and would contribute to destroy H<sub>2</sub> molecules (e.g. Omukai & Nishi 1999), leaving, at the same time, the produced metals as only relevant coolants. This would essentially reproduce the same scenario outlined in Section 3.3. Star formation in purely pristine haloes delayed by radiative or thermal feedback would require more mass to be assembled and atomic cooling to become efficient: due to the higher potential wells, metal spreading in such haloes would probably be less efficient.

Metal mixing due to diffusion processes is taken into account by smoothing metallicities on the kernel. This might be a coarse approximation (see also discussion in Maio et al. 2010, and references therein), but realistic, solid and consistent implementations of (large scale) metal diffusion are currently lacking (approximated attempts are given by e.g. Spitzer 1962; Cowie & McKee 1977; Brookshaw 1985; Sarazin 1988; Monaghan 1992; Cleary & Monaghan 1999; de Avillez & Mac Low 2002; Klessen & Lin 2003; Jubelgas et al.

2004; Monaghan et al. 2005; Wadsley et al. 2008; Greif et al. 2009; Shen et al. 2010). One should expect that large-scale metal mixing could increase the metal-enriched mass which is spread around or falls back to the high-density environments, but no definitive conclusions can be drawn, at the present stage.

The precise cosmological parameters of the  $\Lambda$ CDM model adopted could slightly affect the time-scale of the picture, and significant changes in the background cosmological frame could have some impact, as structure formation could be significantly shifted in redshift. None the less, the global trends (e.g. see Maio et al. 2009) are likely to be recovered.

To conclude, we can state that

- (i) metal pollution is a very efficient process and the critical metallicity is easily reached in less than  $\sim 10^8 \text{ yr}$ ;
- (ii) the PopII regime is, in general, the dominant regime of star formation;
- (iii) the PopIII regime is expected to survive in isolated environments or in the outskirts of star-forming haloes;
- (iv) metal pollution follows an ‘inside-out’ mode and early metals are spread far away from their birth sites, even outside the virial radius;
- (v) the inside-out mode leads metal pollution in closeby star-forming haloes, inducing ‘gravitational enrichment’, while self-enrichment is a negligible process;
- (vi) the coexistence of cold, pristine-gas inflows and of hot, enriched-gas outflows determines turbulence with  $R \sim 10^8\text{--}10^{10}$  and hydro instabilities;
- (vii) different  $Z_{\text{crit}}$  or PopIII IMF alter only slightly these findings.

## ACKNOWLEDGMENTS

We warmly acknowledge the referee, K. Omukai, for his comments on the manuscript. We also acknowledge useful discussions with R. Schneider, N. Yoshida, C. Dalla Vecchia and J. P. Paardekooper. SK acknowledges support from the DFG Cluster of Excellence ‘Origins and Structure of the Universe’ and from the Royal Society Joint Projects Grant JP0869822.

## REFERENCES

- Abel T., Norman M. L., Madau P., 1999, ApJ, 523, 66  
 Abel T., Bryan G. L., Norman M. L., 2000, ApJ, 540, 39  
 Abel T., Bryan G. L., Norman M. L., 2002, Sci, 295, 93  
 Aguirre A., Hernquist L., Schaye J., Katz N., Weinberg D. H., Gardner J., 2001, ApJ, 561, 521  
 Ahn K., Shapiro P. R., 2007, MNRAS, 375, 881  
 Bate M. R., Lodato G., Pringle J. E., 2010, MNRAS, 401, 1505  
 Biffi V., Dolag K., Boehringer H., 2011, MNRAS, doi:10.1111/j.1365-2966.2010.18153.x  
 Bromm V., Loeb A., 2003, Nat, 425, 812  
 Bromm V., Coppi P. S., Larson R. B., 1999, ApJ, 527, L5  
 Bromm V., Yoshida N., Hernquist L., 2003, ApJ, 596, L135  
 Brookshaw L., 1985, Proc. Astron. Soc. Australia, 6, 207  
 Campbell S. W., Lattanzio J. C., 2008, A&A, 490, 769  
 Cen R., 1992, ApJS, 78, 341  
 Cen R., Ostriker J. P., 1992, ApJ, 399, L113  
 Cen R., Riquelme M. A., 2008, ApJ, 674, 644  
 Ciardi B., Ferrara A., 2005, Space Sci. Rev., 116, 625  
 Clark P. C., Glover S. C. O., Klessen R. S., Bromm V., 2011, ApJ, 727, 110  
 Cleary P. W., Monaghan J. J., 1999, J. Comput. Phys., 148, 227  
 Cowie L. L., McKee C. F., 1977, ApJ, 211, 135  
 Crowther P. A., Schnurr O., Hirschi R., Yusof N., Parker R. J., Goodwin S. P., Kassim H. A., 2010, MNRAS, 408, 731

- de Avillez M. A., Mac Low M., 2002, ApJ, 581, 1047  
Dijkstra M., Wyithe J. S. B., 2010, MNRAS, 408, 352  
Dolag K., Vazza F., Brunetti G., Tormen G., 2005, MNRAS, 364, 753  
Dwek E., Cherchneff I., 2011, ApJ, 727, 63  
Dwek E., Galliano F., Jones A. P., 2007, ApJ, 662, 927  
Elmegreen B. G., Scalo J., 2004, ARA&A, 42, 211  
Finlator K., Oppenheimer B. D., Davé R., 2011, MNRAS, 410, 1703  
Galli D., Palla F., 1998, A&A, 335, 403  
Gnedin N. Y., 1998, MNRAS, 294, 407  
Grassi T., Krstic P., Merlin E., Buonomo U., Piovan L., Chiosi C., 2010, preprint (arXiv:1012.1142)  
Greif T. H., Glover S. C. O., Bromm V., Klessen R. S., 2009, MNRAS, 392, 1381  
Greif T. H., Glover S. C. O., Bromm V., Klessen R. S., 2010, ApJ, 716, 510  
Gunn J. E., Gott J. R. I., 1972, ApJ, 176, 1  
Haiman Z., Abel T., Rees M. J., 2000, ApJ, 534, 11  
Hasegawa K., Umemura M., Susa H., 2009, MNRAS, 395, 1280  
Iliev I. T., Shapiro P. R., Raga A. C., 2005, MNRAS, 361, 405  
Johnson J. L., Khochfar S., Greif T. H., Durier F., 2011, MNRAS, 410, 919  
Jubelgas M., Springel V., Dolag K., 2004, MNRAS, 351, 423  
Karlsson T., Johnson J. L., Bromm V., 2008, ApJ, 679, 6  
Katz N., 1992, ApJ, 391, 502  
Katz N., Gunn J. E., 1991, ApJ, 377, 365  
Katz N., Weinberg D. H., Hernquist L., 1996, ApJS, 105, 19  
Kawata D., Gibson B. K., 2003, MNRAS, 340, 908  
Kitayama T., Yoshida N., 2005, ApJ, 630, 675  
Klessen R. S., Lin D. N., 2003, Phys. Rev. E, 67, 046311  
Kobayashi C., 2004, MNRAS, 347, 740  
Komatsu E. et al., 2011, ApJS, 192, 18  
Lia C., Portinari L., Carraro G., 2002a, MNRAS, 335, 864  
Lia C., Portinari L., Carraro G., 2002b, MNRAS, 330, 821  
Maio U., Dolag K., Meneghetti M., Moscardini L., Yoshida N., Baccigalupi C., Bartelmann M., Perrotta F., 2006, MNRAS, 373, 869  
Maio U., Dolag K., Ciardi B., Tornatore L., 2007, MNRAS, 379, 963  
Maio U., Ciardi B., Yoshida N., Dolag K., Tornatore L., 2009, A&A, 503, 25  
Maio U., Ciardi B., Dolag K., Tornatore L., Khochfar S., 2010, MNRAS, 407, 1003  
Maio U., Koopmans L. V. E., Ciardi B., 2011, MNRAS, doi:10.1111/j.1745-3933.2010.01001.x  
Monaghan J. J., 1992, ARA&A, 30, 543  
Monaghan J. J., Huppert H. E., Worster M. G., 2005, J. Comput. Phys., 206, 684  
Mosconi M. B., Tissera P. B., Lambas D. G., Cora S. A., 2001, MNRAS, 325, 34  
O'Shea B. W., Norman M. L., 2007, ApJ, 654, 66  
Omukai K., Nishi R., 1999, ApJ, 518, 64  
Omukai K., Tsuribe T., Schneider R., Ferrara A., 2005, ApJ, 626, 627  
Oppenheimer B. D., Davé R., Kereš D., Fardal M., Katz N., Kollmeier J. A., Weinberg D. H., 2010, MNRAS, 406, 2325  
Papovich C., Finkelstein S. L., Ferguson H. C., Lotz J. M., Giavalisco M., 2010, MNRAS, doi:10.1111/j.1365-2966.2010.17965.x  
Peebles P. J. E., 1974, ApJ, 189, L51  
Raiteri C. M., Villata M., Navarro J. F., 1996, A&A, 315, 105  
Ricotti M., Ostriker J. P., 2004, MNRAS, 350, 539  
Ricotti M., Gnedin N. Y., Shull J. M., 2001, ApJ, 560, 580  
Sarazin C. L., 1988, X-Ray Emissions from Clusters of Galaxies. Cambridge Univ. Press, Cambridge, p. 76  
Saslaw W. C., Zipoy D., 1967, Nat, 216, 976  
Scannapieco E., Schneider R., Ferrara A., 2003, ApJ, 589, 35  
Scannapieco C., Tissera P. B., White S. D. M., Springel V., 2005, MNRAS, 364, 552  
Schaefer D., 2002, A&A, 382, 28  
Schneider R., Omukai K., 2010, MNRAS, 402, 429  
Schneider R., Ferrara A., Salvaterra R., Omukai K., Bromm V., 2003, Nat, 422, 869  
Shen S., Wadsley J., Stinson G., 2010, MNRAS, 407, 1581  
Spitzer L., 1962, Physics of Fully Ionized Gases, 2nd edn. Interscience, New York  
Springel V., 2005, MNRAS, 364, 1105  
Springel V., Hernquist L., 2003, MNRAS, 339, 289  
Stacy A., Bromm V., Loeb A., 2010, ApJ, preprint (arXiv:1011.4512)  
Suda T., Fujimoto M. Y., 2010, MNRAS, 405, 177  
Tornatore L., Borgani S., Dolag K., Matteucci F., 2007a, MNRAS, 382, 1050  
Tornatore L., Ferrara A., Schneider R., 2007b, MNRAS, 382, 945  
Tseliakhovich D., Hirata C., 2010, Phys. Rev. D, 82, 083520  
Tseliakhovich D., Barkana R., Hirata C., 2010, preprint (arXiv:1012.2574)  
Valdarnini R., 2011, A&A, 526, A158  
Wadsley J. W., Veeravalli G., Couchman H. M. P., 2008, MNRAS, 387, 427  
Weinmann S. M., Lilly S. J., 2005, ApJ, 624, 526  
Whalen D., van Veelen B., O'Shea B. W., Norman M. L., 2008, ApJ, 682, 49  
Whalen D., Hueckstaedt R. M., McConkie T. O., 2010, ApJ, 712, 101  
Wise J. H., Abel T., 2008, ApJ, 685, 40  
Woosley S. E., Weaver T. A., 1995, ApJS, 101, 181  
Yoshida N., 2006, New Astron. Rev., 50, 19  
Yoshida N., Abel T., Hernquist L., Sugiyama N., 2003, ApJ, 592, 645  
Yoshida N., Omukai K., Hernquist L., 2007, ApJ, 667, L117  
Yoshida N., Omukai K., Hernquist L., 2008, Sci, 321, 669

This paper has been typeset from a TeX/LaTeX file prepared by the author.